

Influence of Porous and Electronic Structure of Carbon Materials on the Supercapacitor Capacitance

I. BORDUN^{a,b,*}, Z. KOHUT^{a,b}, E. SZYMCZYKIEWICZ^a,
M. MALOVANYI^b, N. NAHURSKYI^b AND N. POKLADOK^b

^a*Czestochowa University of Technology, J.H. Dąbrowskiego 42-201 Częstochowa, Poland*

^b*Lviv Polytechnic National University, S. Bandera 12, 79013 Lviv, Ukraine*

Doi: [10.12693/APhysPolA.147.241](https://doi.org/10.12693/APhysPolA.147.241)

*e-mail: ihor.bordun@pcz.pl

The article discusses the relationship between the porous and electronic structure of nanoporous bio-carbon materials and their electrochemical behavior in an alkaline electrolyte. Based on the results of X-ray diffraction and adsorption–desorption gas porometry, it was found that the synthesis temperature of the carbon material affects both the content of the graphite phase and the parameters of the carbon porous structure. The impedance behavior of supercapacitor electrodes made of synthesized carbons at different bias voltages is analyzed. For the obtained Nyquist diagrams, equivalent electrical circuits are constructed based on the modified de Levie model. The influence of the synthesis temperature on the position of the Fermi level is determined by the nature of the change of the minimum in the volt–farad dependence of the spatial charge region capacitance. It has been shown that the shift of the Fermi level to the energy region with a high density of delocalized electron states helps unlock the Helmholtz layer’s capacity and, as a result, the specific capacitance of the carbon material increases.

topics: supercapacitor (SC), carbon, specific capacitance, Nyquist diagram

1. Introduction

The rapid growth of global energy consumption necessitates the search for new energy generation, conversion, and storage sources. Among them, electrochemical energy storage devices such as batteries and supercapacitors (SCs) can be distinguished. Highly porous carbon-based materials play a key role in these devices [1, 2]. The production of carbon materials involves methods such as physical or chemical activation of carbon-containing precursors [3], template synthesis [4], or the synthesis of supramolecular compounds [5].

When activated carbon (AC) is employed as active electrode material in SCs, the primary parameter characterizing SCs becomes the specific capacitance in a chosen type of electrolyte. Many studies attempt to correlate the specific surface area with the specific capacitance. Nevertheless, the results are often contradictory. For instance, in [6], the authors demonstrated that the specific capacitance of the investigated types of carbon materials increases linearly with the increase in the specific surface area. In [7], 13 types of AC synthesized via different methods were studied. Although no strict linear relationship between the specific surface area and the specific capacitance was established, the

authors introduced the concept of a “critical” pore size for each electrolyte. Similarly, in [8], the authors do not report a direct correlation between the specific surface area and the specific capacitance of carbon materials. The studies presented in [9, 10] propose a model that integrates the porous and electronic structures, which affects the formation of the electric double layer (EDL) on the carbon electrode surface.

The capacitance of a non-metallic SC electrode is the sum of three capacitances, connected in series: (i) the capacitance of the space charge region (SCR) in a solid body, C_{SC} , (ii) the Helmholtz capacitance, C_H , and (iii) the Gouy–Chapman capacitance, C_G . In aqueous electrolyte solutions, $C_G \gg C_H$, so the total capacitance can be calculated as

$$C = \frac{C_H C_{SC}}{C_H + C_{SC}}. \quad (1)$$

Unlocking the Helmholtz capacitance C_H is facilitated by an increase in the capacitance C_{SC} , which is associated with the density of electronic states at the Fermi level [11],

$$C_{SC} = e \sqrt{\varepsilon \varepsilon_0 D(F)}, \quad (2)$$

where e is the electron charge, ε — dielectric permittivity of the medium, ε_0 — electric constant, $D(F)$ — density of electronic states at the Fermi level.

The issue of unlocking the Helmholtz capacitance is critical for carbon electrodes due to the relatively large Debye screening radius in carbon materials [9]. Therefore, our study aimed to synthesize AC with a similar pore distribution but varying specific surface areas, determine its specific capacitance, and analyze the influence of the carbon material's electronic structure on this capacitance.

2. Experimental part

2.1. Synthesis of carbon materials

Agricultural waste, specifically pelletized wheat straw, was selected as the raw material for synthesis, which was conducted in two stages. In the first stage, the wheat straw pellets underwent pre-pyrolysis. A crucible containing the pellets was placed in a furnace and subjected to pre-pyrolysis at 400°C for 90 min. In the second stage, the obtained char was added to an aqueous solution of KOH and kept for 24 h. The mass ratio of char to KOH was 1:3. The dried powder was heated in a furnace at 10°C/min to the synthesis temperature and maintained at this temperature for 90 min. The synthesis temperatures were 600°C, 700°C, and 800°C. The synthesized carbon samples are denoted in the text as C600, C700, and C800, respectively.

2.2. Methods of experimental investigation

The macroscopic structure of the synthesized carbon materials was studied using a Phenom ProX scanning electron microscope. The microstructure was analyzed through X-ray diffraction using a DRON-3 diffractometer with monochromatized Cu K_{α} -radiation ($\lambda = 0.1542$ nm) over the diffraction angle range $2\theta = 10^{\circ}$ – 80° .

The porous structure of the synthesized samples was investigated using the nitrogen adsorption/desorption method at its boiling point with a Quantachrome NOVAtouch LX2 porometer.

The SC electrodes were fabricated using carbon particles ground to 40–63 μm . Polyvinylidene fluoride (PVDF) was used as the binding agent, with a mass ratio of AC to PVDF of 19:1. The active material was applied to a nickel mesh and pressed with a hydraulic press at a force of 500 N/cm².

The specific capacitance of the synthesized AC in a 30% aqueous KOH solution was determined based on galvanostatic charge/discharge measurements [10].

Impedance studies of AC were conducted in a three-electrode cell with a silver chloride reference electrode over the frequency range of 10^{-2} – 10^6 Hz using an AUTOLAB PGSTAT-100 impedance spectrometer.

3. Results and discussion

3.1. Structural investigations

Scanning electron microscope (SEM) images of all synthesized samples (Fig. 1a–c) clearly demonstrate the macroscopic porous structure of AC.

In all cases, the carbon particles retain the morphological features of the raw material — here, wheat straw — regardless of the synthesis temperature. However, the synthesis temperature does influence the carbon material microstructure, as observed via X-ray diffraction. As shown in Fig. 2, all samples consist of an amorphous phase along with an additional identified phase of silicon dioxide SiO₂. Furthermore, the diffractograms of samples C600 and C700 exhibit a distinct peak corresponding to the reflection from the (002) graphite plane ($d_{(002)} = 0.335$ nm).

Analysis of the broad diffuse maximum for sample C600 revealed the interlayer distances of $d \approx 0.42$ nm (reflection from the (002) plane). This indicates significant disorder in the amorphous carbon phase due to weakened Van der Waals interactions, caused by the azimuthal misorientation of adjacent graphene layers relative to each other. The diffractogram of sample C700 also exhibits a broad maximum corresponding to the interlayer distances of $d \approx 0.41$ nm. As seen in Fig. 2, the diffractogram of sample C800 shows a significant increase in background scattering at lower diffraction angles, characteristic of microporous materials. The angular position of the main maximum at $2\theta \approx 19^{\circ}$ corresponds to the interlayer distance

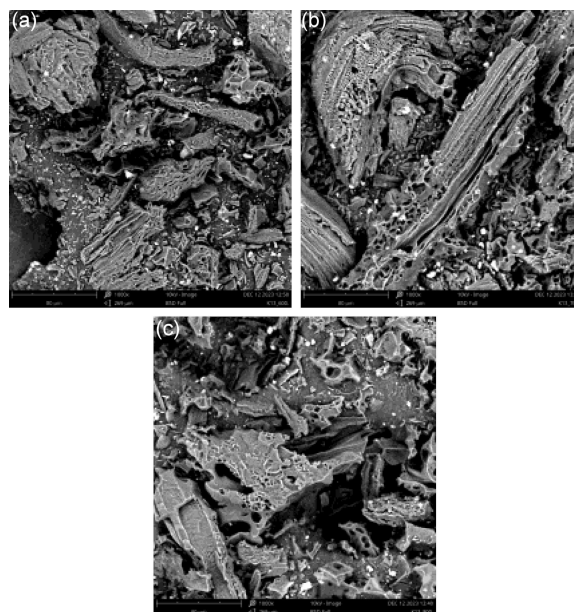


Fig. 1. SEM images of synthesized carbon materials: C600 (a), C700 (b), and C800 (c).

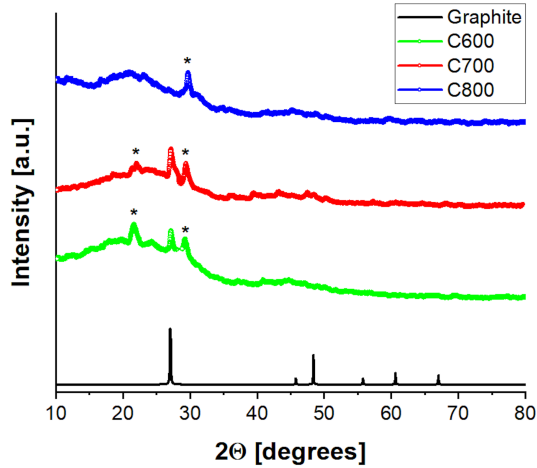


Fig. 2. X-ray diffractograms of synthesized carbon materials; * — identified SiO_2 peaks.

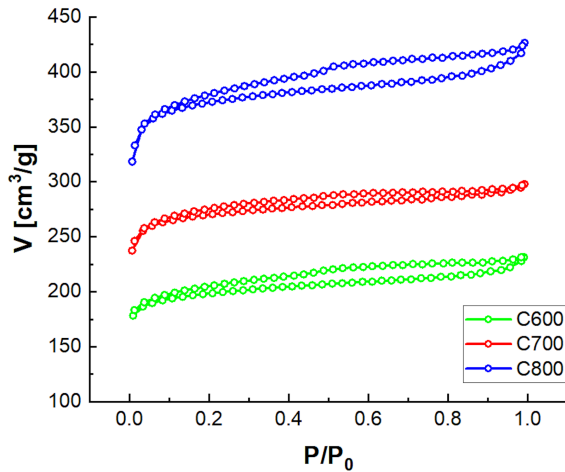


Fig. 3. Nitrogen adsorption/desorption isotherms of synthesized carbon materials.

of $d \approx 0.47$ nm. The absence of a distinct graphite peak at $2\theta \approx 27^\circ$ suggests a higher degree of atomic disorder compared to the C600 and C700 samples.

Nitrogen adsorption/desorption isotherms for all synthesized samples are qualitatively similar (Fig. 3). Their shape can be classified as type I isotherms, characteristic of microporous solids [12]. Additionally, all isotherms exhibit H4-type hysteresis [12], indicative of slit-like pores.

The specific surface area and total pore volume were determined using the Brunauer–Emmett–Teller (BET) method [13]. The calculation results are presented in Table I. As evident from the data, increasing the synthesis temperature from 600 to 800°C leads to an increase in both the specific surface area and the specific pore volume of the carbon samples.

Since the isotherms in Fig. 3 are characteristic of microporous samples, the microporous structure parameters were calculated using the t -method [13]

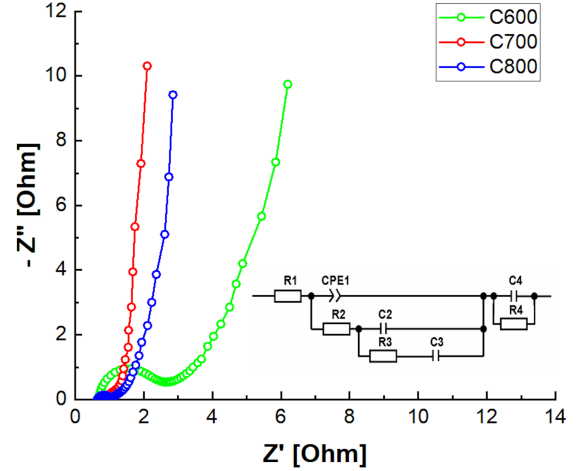


Fig. 4. Nyquist diagrams for synthesized carbon materials (bias voltage $\Delta U = 0$ V). Inset: Equivalent electrical circuit modeling the SC frequency response.

TABLE I

Parameters of porous structure of synthesized carbon materials.

Sample	S_{BET} [m^2/g]	V [cm^3/g]	S_t [m^2/g]	V_t [cm^3/g]
C600	619.5	0.359	589.6	0.299
C700	842.1	0.462	816.0	0.414
C800	1161.7	0.661	1113.9	0.563

(Table I). The results confirm the microporosity of all samples, since the content of mesopores and macropores is negligible.

3.2. Electrochemical studies

Galvanostatic charge–discharge tests at a current density of 1 A/g for SCs based on synthesized carbon materials revealed specific capacitances of 123.4 ± 3.8 F/g for AC C600, 189.5 ± 2.1 F/g for AC C700, and 148.3 ± 2.5 F/g for AC C800. Thus, AC C700 exhibits the highest specific capacitance.

To analyze the influence of carbon's porosity and electronic structure on its electrochemical performance, impedance measurements were conducted and Nyquist plots were constructed over a voltage range from 0.8 to +0.2 V. The typical Nyquist diagrams are shown in Fig. 4.

The obtained Nyquist plots are characteristic of carbon electrodes with charge accumulation in EDL at the electrode/electrolyte interface. For electrodes fabricated from C600, a distinct semicircle in the high-frequency region is observed, associated with Faradaic processes [14]. These processes likely stem from quasi-reversible electrochemical reactions of

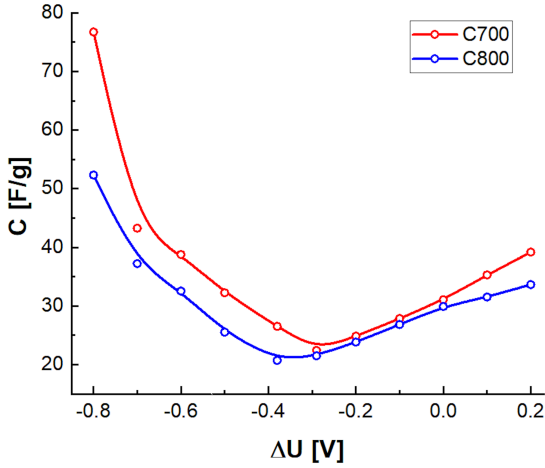


Fig. 5. Voltage–capacitance dependence of specific SCR capacitance in synthesized carbon materials.

reduction oxygen-containing surface groups in alkaline solutions. For C700 and C800, the semicircles in the high-frequency region are smaller, and the Nyquist plots are quite similar.

To gain deeper insights, the Nyquist plots for electrodes fabricated from C700 and C800 were modeled using an equivalent electrical circuit based on a modified de Levie model in the ZView 3.4 software. This modification includes the sequential addition of an R4C4-branch (Fig. 4, inset), representing the resistance and capacitance of the SCR in the carbon material. The model includes a constant phase element CPE1, which accounts for the distributed capacitance due to the porous structural heterogeneity of the carbon.

The specific SCR capacitance $C4$ calculated from the equivalent electrical circuit in Fig. 4, inset, as a function of the applied bias voltage is shown in Fig. 5. The minimum SCR capacitance for C700 occurs at $\Delta U = -0.29$ V, while for C800 it is at $\Delta U = -0.38$ V.

The position of the minimum in the voltage–capacitance dependence determines the chemical potential μ_E of each material in the electrolyte [11]

$$\mu_E = F - e\varphi_S, \quad (3)$$

where F is the position of the Fermi level, φ_S — potential corresponding to the minimum in the $C(\Delta U)$ dependence.

Since the electrolyte is identical for both samples, their electrochemical potentials are equal

$$\mu_{E1} = \mu_{E2}, \quad \text{so} \quad F_1 - e\varphi_{S1} = F_2 - e\varphi_{S2}. \quad (4)$$

From 4, the shift in the Fermi level as a function of the carbon material synthesis temperature can be calculated as

$$F_2 - F_1 = e(\varphi_{S2} - \varphi_{S1}) = e(-0.29 - (-0.38)) = 0.09 \text{ eV}, \quad (5)$$

where the subscript “1” corresponds to C800 and the subscript “2” corresponds to C700.

Thus, for sample C700, the positive shift in the minimum $C(\Delta U)$ graph compared to C800 implies that the Fermi level in C700 is shifted by 0.09 V into an energy region with higher density of electronic states. According to (2), in the carbon material, the density of electronic states determines the SCR capacitance. Consequently, the positive Fermi level shift is an essential factor contributing to the higher specific capacitance of carbon samples with lower specific surface area.

4. Conclusions

The conducted studies revealed a nonlinear relationship between specific capacitance and specific surface area in biocarbon materials synthesized at various temperatures using KOH activation. With the increase in synthesis temperature, the total specific surface area increases; however, the content of the graphite phase decreases, influencing the electronic structure of the synthesized carbon. Analysis of changes in electronic structure based on voltage–capacitance dependences of SCR capacitance showed that, as the synthesis temperature increases from 700 to 800°C, the Fermi level shifts into an energy region with higher density of delocalized electronic states. This shift results in the Helmholtz layer capacitance unblocking by increasing the SCR capacitance in the carbon material. Consequently, the capacitance redistribution occurs within the electric double layer of the supercapacitor, which leads to an increase in the specific capacitance of the carbon material.

References

- [1] G.G. Bizuneh, A.M.M. Adam, J. Ma, *Battery Energy* **2**, 20220021 (2023).
- [2] P. Trihutomo, P. Puspitasari, M. Nabiałek, *Acta Phys. Pol. A* **144**, 395 (2023).
- [3] M.A. Yahya, Z. Al-Qodah, C.W.Z. Ngah, *Renew. Sustain. Energy Rev.* **46**, 218 (2015).
- [4] C. Wang, B. Yan, J. Zheng et al., *Adv. Powder Mater.* **1**, 100018 (2022).
- [5] V. Ptashnyk, I. Bordun, D. Całus, P. Chabecki, V. Maksymych, M. Malovanyy, A. Borysiuk, Y. Kulyk, *Appl. Phys. A* **128**, 569 (2022).
- [6] E. Taer, A. Agus, R. Farma et al., *J. Phys. Conf. Ser.* **1116**, 032040 (2018).
- [7] C. Young, J. Lin, J. Wang et al., *Chem. Eur. J.* **24**, 6127 (2018).

- [8] B. Lobato, L. Suárez, L. Guardia, T.A. Centeno, *Carbon* **122**, 234 (2017).
- [9] R.Y. Shvets, I.I. Grygorchak, A.K. Borysyuk, S.G. Shvachko, A.I. Kondyr, V.I. Baluk, A.S. Kurepa, B.I. Rachiy, *Phys. Solid State* **56**, 2021 (2014).
- [10] V. Ptashnyk, I. Bordun, V. Pohrebennyk, J. Takosoglu, M. Sadova, *Przeegląd Elektrotech.* **2018**, 186 (2018).
- [11] H. Gerischer, R. McIntyer, D. Scherson, W. Storck, *J. Phys. Chem.* **91**, 1930 (1987).
- [12] M. Thommes, K. Kaneko, A.V. Neimark, J.P. Olivier, F. Rodriguez-Reinoso, J. Rouquerol, K.S.W. Sing, *Pure Appl. Chem.* **87**, 1051 (2015).
- [13] J. Rouquerol, F. Rouquerol, P. Llewellyn, G. Maurin, K.S.W. Sing, *Adsorption by Powders and Porous Solids: Principles, Methodology and Applications* 2nd ed., Academic Press, New York 2013.
- [14] B.E. Conway, *Electrochemical Supercapacitors. Scientific Fundamentals and Technological Applications*, Kluwer Academic/Plenum Publishers, New York 1999.